JACS Au
AN OPEN ACCESS JOURNAL OF THE AMERICAN CHEMICAL SOCIETY

pubs.acs.org/jacsau
Article

Spatiotemporal Organization of Functional Cargoes by Light-Switchable Condensation in *Escherichia coli* Cells

Fang Pan, Han Zu, Ya-Jiao Zhu, Zhi-Gang Qian,* and Xiao-Xia Xia*

Cite This: *JACS Au* 2024, 4, 1480−1488
Read Online

ACCESS | Metrics & More | Article Recommendations | Supporting Information

ABSTRACT: Biomolecular condensates are dynamic subcellular compartments that lack surrounding membranes and can spatiotemporally organize the cellular biochemistry of eukaryotic cells. However, such dynamic organization has not been realized in prokaryotes that naturally lack organelles, and strategies are urgently needed for dynamic biomolecular compartmentalization. Here we develop a light-switchable condensate system for on-demand dynamic organization of functional cargoes in the model prokaryotic *Escherichia coli* cells. The condensate system consists of two modularly designed and genetically encoded fusions that contain a condensation-enabling scaffold and a functional cargo fused to the blue light-responsive heterodimerization pair, iLID and SspB, respectively. By appropriately controlling the biogenesis of the protein fusions, the condensate system allows rapid recruitment and release of cargo proteins within seconds in response to light, and this process is also reversible and repeatable. Finally, the system is demonstrated to dynamically control the subcellular localization of a cell division inhibitor, SulA, which enables the reversible regulation of cell morphologies. Therefore, this study provides a new strategy to dynamically control cellular processes by harnessing light-controlled condensates in prokaryotic cells.

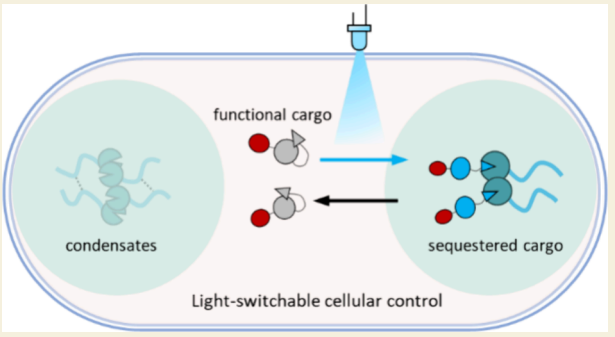

KEYWORDS: *biomolecular condensates, optogenetics, dynamic regulation, cellular engineering, synthetic biology*

INTRODUCTION

Biomolecular condensates are microscale subcellular compartments that lack surrounding membranes but function to concentrate proteins and/or nucleic acids in eukaryotic cells.[1−3] These condensates play important roles in regulation of cellular processes, such as subcellular organization of biochemical reactions, gene regulation, and stress response.[4−7] Typically, the condensates comprise two types of components: the "scaffolds" that drive the condensate assembly and the biomolecular "clients" that selectively partition into the condensates to endow biological functions.[8] Inspired by this organization principle of natural condensates, various scaffold molecules, such as intrinsically disordered proteins,[9] folded-domain repeat proteins,[10] or RNA,[11] have been engineered to construct synthetic condensates with on-demand functions in eukaryotic cells.[12] However, the creation of synthetic condensates in prokaryotes has been underexplored, which is partially attributed to the aggregation-prone characteristics of scaffold proteins and the distinctly different cellular environments between prokaryotes and eukaryotes.

Unlike eukaryotic cells, prokaryotes are relatively small in size (submicron to a few microns) and highly crowded within intracellular environments, which make it more challenging to assemble functional condensates.[13] To tackle this problem, our group has recently rewired intrinsically disordered structural proteins for direct fusion with client enzymes for compartmentalized biosynthesis in the model prokaryotic bacterium *Escherichia coli*.[13,14] As direct fusions may reduce the activities of cargo enzymes, peptide−peptide interaction pairs such as RIDD−RIAD have attracted attention for the specific recruitment of appropriately tagged enzymes into the condensates for improved biosynthesis in *E. coli*.[15,16] Intriguingly, polypeptide domains that bind specific DNA sequences have also been utilized to recruit plasmid DNA into synthetic condensates for transcriptional regulation in *E. coli*.[17] Despite these successes in metabolic and cellular engineering, reversible and repeatable recruitment and release of clients remain to be addressed for native-like dynamic regulation of cellular functions,[17,18] which is crucial for enhancing cell fitness and robustness.

Light-controlled optogenetic tools are intriguing for dynamic regulation[19,20] due to their precise control over protein−protein interactions in a spatiotemporal and reversible manner.

Received: January 5, 2024
Revised: March 12, 2024
Accepted: March 25, 2024
Published: March 29, 2024

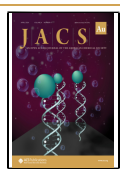

Scheme 1. Schematic Diagram of Light-Activated Synthetic Condensate (LASC) System for Reversible Client Recruitment and Release[a]

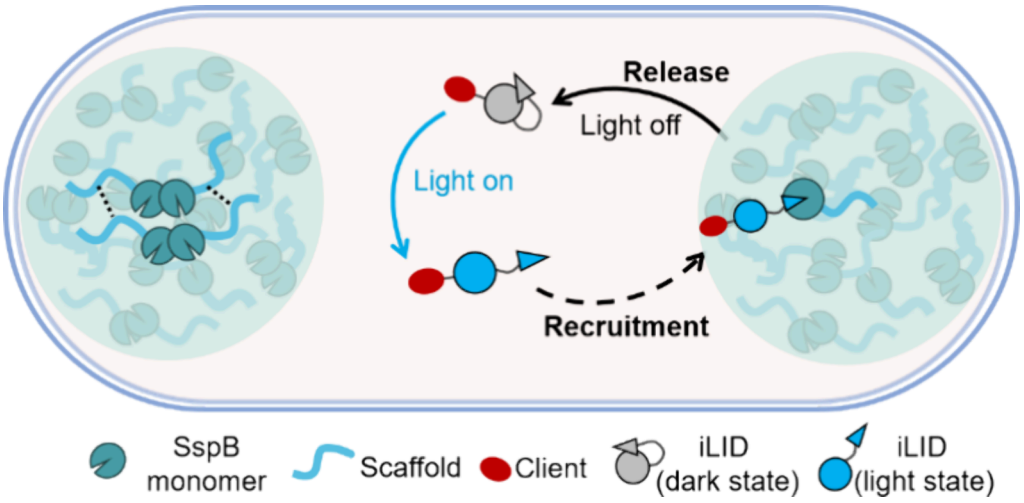

[a]The blue light-responsive heterodimerization pair, iLID−SspB, is used for reversible light control. Synthetic condensates are formed via the multivalent interactions of SspB-tagged scaffold protein. A client protein of interest fused with photoactivatable iLID is recruited to the condensates upon blue light illumination and released back into the bulk cytoplasmic milieu by switching off the light. Notably, homodimerization of SspB facilitates phase separation of the SspB-tagged scaffold protein, despite the fact that SspB alone is insufficient for driving phase separation into condensates.

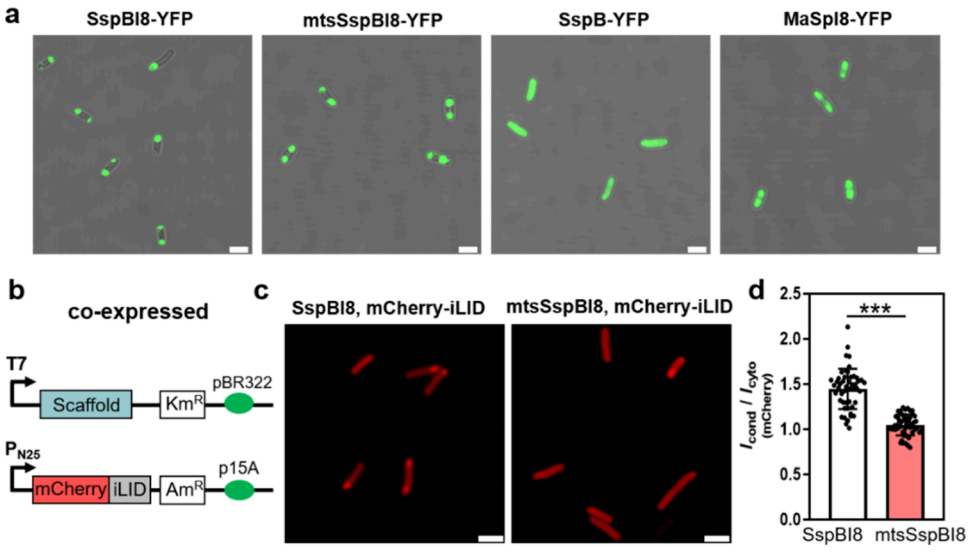

Figure 1. Modular design of scaffold and client proteins for synthetic condensate formation in cells. (a) The merged fluorescence and bright-field microscopy images of *E. coli* cells expressing yellow fluorescent protein (YFP)-tagged scaffold. Subcellular localization of the YFP fluorescence indicated formation of condensates at the cell poles for SspBI8-YFP and mtsSspBI8-YFP. Scale bars: 2.5 μm. (b) Illustration of genetic constructs for coexpression of the scaffold and client proteins from two compatible plasmids, differing in replication origins (pBR322 or p15A origin), antibiotic resistance genes (Km^R or Am^R), and promoters for transcriptional control (the IPTG-inducible T7 promoter or the constitutive P_{N25} promoter). (c) Confocal fluorescence images of the cells coexpressing client mCherry-iLID and scaffold SspBI8 or mtsSspBI8. Note that the scaffolds formed condensates at the cell poles, and the fluorescence shows the subcellular distribution of the mCherry client without blue light irradiation. Scale bars: 2.5 μm. (d) Quantification of the ratio of the mCherry fluorescence intensity of condensates to that of the bulk cytosol (I_{cond}/I_{cyto}). Data are presented as the mean ± s.d. (n = 50 cells). Statistical significance was determined using an unpaired t-test for P values (***P < 0.001). All the cells were grown in rich LB medium, induced with 25 μM IPTG for scaffold expression, and sampled at 6 h postinduction for imaging. Data in (a), (c), and (d) are representative of n = 3 independent experiments.

As optogenetic molecules are relatively large in molecular weights and prone to aggregation upon overexpression in prokaryotic cells, fusion expression of optogenetic molecules with scaffolding and client proteins often leads to the formation of insoluble and inactive aggregates,[9,18,21,22] which adversely affects the functioning of the resulting condensates and the realization of reversible and repeatable regulation. To address this challenge, here, we propose a modular framework for the organization of synthetic condensates by decoupling condensate formation and client recruitment/release (Scheme 1). Briefly, two modularly designed and genetically encoded fusions are constructed that contain a condensation-enabling scaffold and a functional cargo, respectively, fused to a blue light-responsive heterodimerization pair. Specifically, the

https://doi.org/10.1021/jacsau.4c00017
JACS Au 2024, 4, 1480−1488

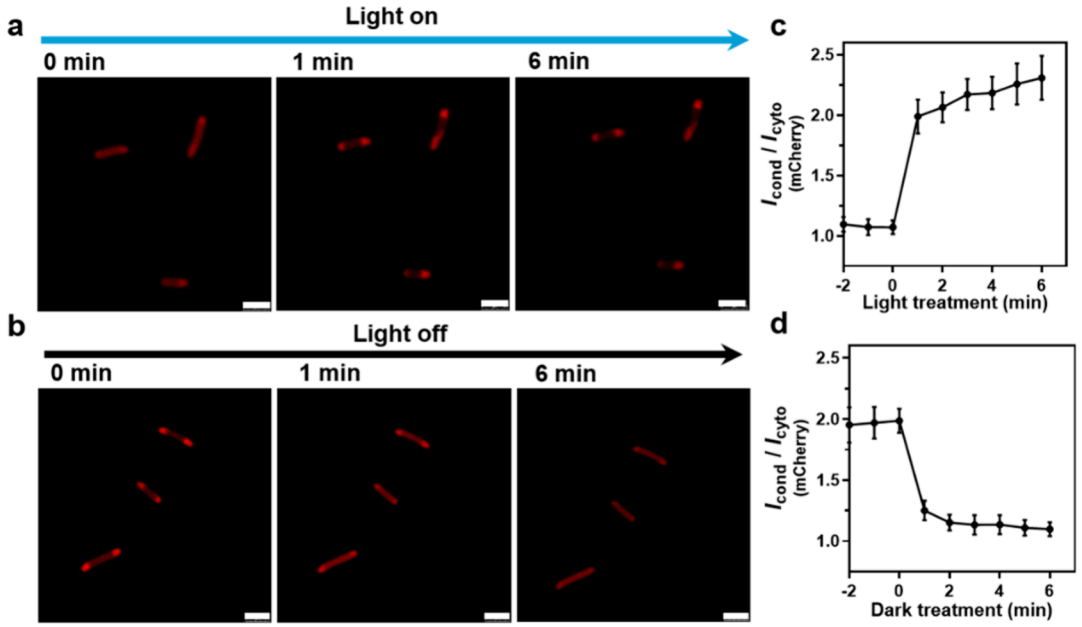

Figure 2. Kinetics of client recruitment and release from synthetic condensates. Representative time-lapse fluorescence microscopy images of the *E. coli* cells co-expressing mtsSspBI8 and mCherry-iLID under 488 nm blue-light irradiation (a) or dark treatment (b). The mCherry fluorescence indicates subcellular localization of mCherry-iLID within the cells. Images were taken every 1 min for quantification of the fluorescence intensities. Scale bars: 2.5 μm. (c, d) Quantification of the ratio of the mCherry-iLID fluorescence intensity of condensates to that of the bulk cytosol (I_{cond}/I_{cyto}) of cells from 4 fields of view in (a) and (b), respectively. The ratio data in (c) and (d) are presented as mean ± s.d. (n = 10 cells). The data in parts a–d are representative of n = 3 independent experiments.

improved light inducible dimer (iLID) and its adaptor protein (SspB) are chosen due to their multiple desirable traits such as appropriate binding affinity, fast activation and reversion kinetics, and tolerance to both N- and C-terminal fusions.[20,23] To this end, we first made genetic constructs encoding a light-activated synthetic condensate (LASC) system for dynamic control of the sequestration/release of clients in *E. coli* cells. Then we evaluated the kinetics of client recruitment and release in response to blue light and found its fast, reversible and repeatable responsive features. Finally, this LASC system was demonstrated to dynamically regulate cell morphologies by light-switchable organization of the key cell division inhibitor SulA.

RESULTS AND DISCUSSION

This study was initiated with the design of suitable scaffold proteins that dictate the formation of subcellular condensates. We have recently revealed that a series of spider silk-like proteins with varying numbers of consensus peptide sequences were able to form liquid-like condensates in *E. coli* cells, and their liquid–liquid phase separation behavior was dependent on the silk protein molecular weights.[13] Here we chose a low-molecular-weight silk protein MaSpI8 as the scaffold for C-terminal fusion to the adaptor protein SspB (Micro), which naturally forms a strong homodimer,[24] and the resulting fusion protein was termed SspBI8. In another tripartite fusion construct mtsSspBI8, the membrane-targeting sequence (mts)[25] derived from the *E. coli* MinD was fused to the N-terminus of SspBI8, with an attempt to provide anchoring nucleation sites that may potentially aid the formation of phase-separated condensates. To visualize the expression and localization of the above two scaffold proteins in recombinant *E. coli* cells, the yellow fluorescent protein (YFP) was additionally fused at the C-terminus of each construct (Figure 1a). Notably, fusion constructs were also made by similarly labeling the adaptor protein SspB (Micro) and silk protein MaSpI8 with YFP, leading to SspB-YFP and MaSpI8-YFP that served as controls. Confocal imaging revealed that the expression of SspBI8-YFP or mtsSspBI8-YFP as fluorescent condensates spatially localized near the pole regions of the *E. coli* cells grown in LB liquid medium, while the control SspB-YFP was uniformly distributed through the cytosol and MaSpI8-YFP could cause only weak phase separation. These results indicate that the dimerization of SspB can enhance the homotypic interactions of MaSpI8 protein chains, thus driving phase separation and condensate formation. Besides, the synthetic condensates emerged and matured with the induced expression of the scaffold proteins in a time-dependent manner (Figure S1). Interestingly, the condensates appeared as a relatively small droplet-like assembly at the bacterial cell poles (nucleoid excluded with high curvatures), which was hypothetically attributed to the locally enhanced scaffold protein concentration. It appeared that the abilities of the scaffold proteins to form condensed phases varied, which may be attributed to the differential strengths of homotypic molecular interactions that drive protein condensation; yet the translation rates and overall production levels of these scaffold proteins in recombinant cells may also play roles in condensate formation. To exclude the interference of YFP fusion in condensate formation, we also characterized the SspBI8- or mtsSspBI8-expressing cells by transmission electron microscopy (TEM). Consistent with the observation from fluorescence microscopy, the condensates were clearly observed at the cell poles (Figure S2). In addition, we explored whether the medium richness would affect condensate formation. To this end, we used a minimal salt glucose medium to grow the cells and express the scaffold proteins to examine their subcellular localization (Figure S3). Notably, subcellular localization of these scaffolds

https://doi.org/10.1021/jacsau.4c00017
JACS Au 2024, 4, 1480–1488

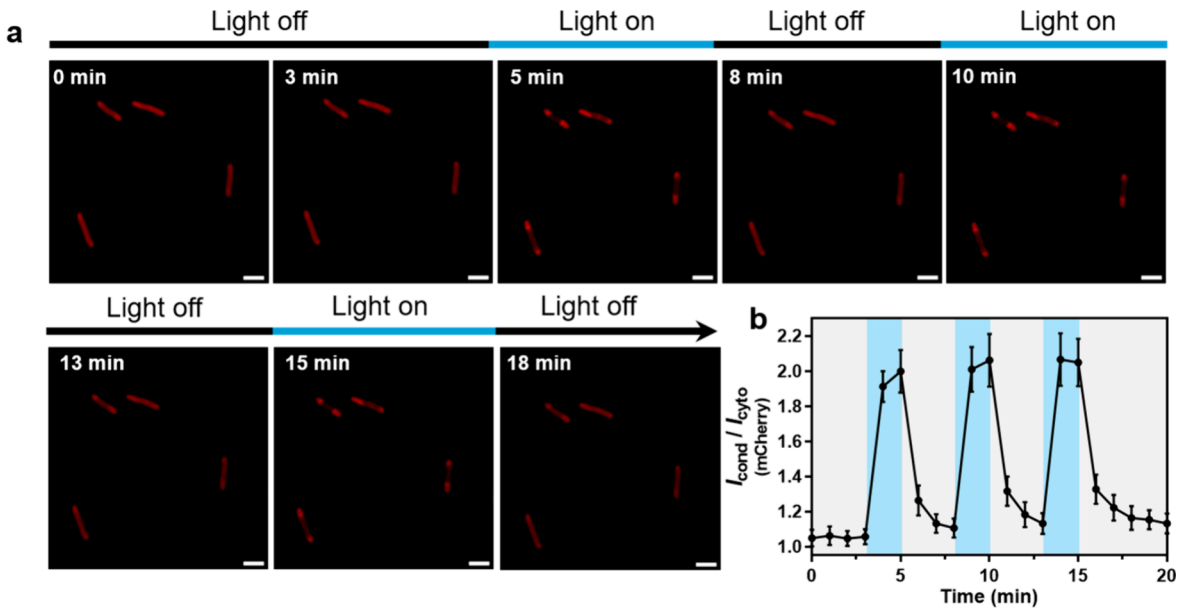

Figure 3. Reversible client recruitment and release in a repeatable manner. (a) Representative time-lapse images of the recombinant *E. coli* cells under 3 cycles of 2 min of blue-light illumination and 3 min darkness. For comprehensive assay of the ground and recovery states, the cells were monitored for additional 3 min before the cyclic tests and 2 min after the tests and imaged every 1 min for a total time of 20 min; for clarity, only the images at the blue-light switching times are shown. Scale bars: 2.5 μm. (b) Ratio of the mCherry-iLID fluorescence intensity of condensates to that of the bulk cytosol (I_{cond}/I_{cyto}) of cells from 3 fields of view in (a). Data are presented as mean ± s.d. (n = 10 cells), and the blue shadings indicate 2 min pulses of the 488 nm blue light illumination. Data in parts a and b are representative of n = 3 independent experiments.

was essentially the same as that observed for the cells grown in the rich LB medium (Figure 1a), suggesting that the medium richness may not affect condensate formation under the experimental conditions in our study.

Next we chose the monomeric red fluorescent protein (mCherry) as a model cargo and fused it to the N-terminus of photoreceptor iLID. The resulting mCherry-iLID fusion was then co-expressed with either the scaffold protein SspBI8 or mtsSspBI8 in recombinant *E. coli* cells (Figure 1b). Notably, the two scaffold proteins were appreciably expressed at comparable levels (17−21% of total cellular proteins), whereas the client mCherry-iLID was moderately expressed at 10−13% of total cellular proteins (Figure S4). To investigate the intracellular distribution of the mCherry-iLID protein without light treatment, the two groups of recombinant cells were cultured in darkness for 6 h and taken for confocal imaging. In the cells with the expression of SspBI8, an obvious enrichment of mCherry fluorescence was observed in the cell pole regions. In contrast, the mCherry signal was evenly distributed throughout the cells with expression of mtsSspBI8 (Figure 1c). By quantifying the ratio of mCherry fluorescence in the pole region to the bulk cytosol, we observed a 1.5-fold higher partition coefficient for the SspBI8-expressing cells than that of the cells expressing mtsSspBI8 (Figure 1d). This implied interactions between the mCherry-iLID and SspBI8 fusion proteins were strong enough to cause nonspecific recruitment, which is undesirable for the development of stringent and dynamic regulation system. It should be noted that the issue of such nonspecific interactions are rather challenging to tackle both *in vivo* and *in vitro* reconstitutions.[26,27] Surprisingly, the daunting issue has been significantly alleviated by incorporation of mts into the SspBI8 scaffold, possibly due to that membrane localization of the scaffold reduced the chances of contact with the mCherry-iLID client and the nonspecific heterotypic molecular interactions. Therefore, mtsSspBI8 was used as the scaffold protein in the following studies.

Then we analyzed the *E. coli* cells co-expressing the scaffold protein mtsSspBI8 and client mCherry-iLID by TEM. As expected, clear formation of condensed phases was observed, and the synthetic condensates were localized at the cell pole regions with a condensate area of ∼0.7 μm^2 (Figure S5). To determine whether the client mCherry-iLID could be recruited into the mtsSspBI8 condensates upon blue light illumination, we illuminated the recombinant cells *in situ* with a 488 nm laser light and monitored localization of the mCherry fluorescence (Figure 2a). Prior to blue light exposure, the red fluorescence was uniformly distributed throughout the cell. Upon blue light illumination, the fluorescence was largely translocated to the cell poles within a minute. Importantly, such translocation of the client protein could be well maintained with the presence of blue light irradiation for at least 6 min. Furthermore, we examined whether the client protein could be released from the synthetic condensates at the cell poles. By switching off the blue light, we observed that the previously recruited mCherry-iLID rapidly diffused into the bulk cytosol within minutes (Figure 2b). By quantifying the ratio of mCherry fluorescence in condensates and cytoplasm with continuous blue light or dark conditions (Figure 2c,d), half-times of the client recruitment and release were roughly estimated to be 33.1 ± 11.2 and 22.3 ± 7.2 s, respectively. This fast kinetics coincided well with the response time scale of the binding and dissociation of the iLID system.[20] Furthermore, we verified that the mCherry-labeled iLID did not form condensates (Figure S6a) or affect phase separation of the scaffold protein MaSpI8-YFP in cells (Figure S6b). Taken together, it is confirmed that the blue light-triggered interaction of iLID to the formed condensates gave rise to the cargo recruitment.

https://doi.org/10.1021/jacsau.4c00017
JACS Au 2024, 4, 1480−1488

Then we studied whether the cells co-expressing mtsSspBI8 and mCherry-iLID can support reversible client recruitment and release. To this end, we treated the cells with blue light irradiation for 1 min, followed by 1 min darkness. As expected, the cells demonstrated reversible client recruitment and release in the 1 min light on/off cycle (Figure S7), whereas the control cells lacking the photoreceptor iLID could not realize the light-switchable organization (Figure S8). These results suggested that the interaction between iLID and SspB is required for the dynamic recruitment and release and that the formation of mtsSspBI8 condensates did not interfere with the binding capability of SspB to the iLID in response to blue light, which enabled the rapid light-controlled recruitment and release of the client. Furthermore, we explored whether the reversible client recruitment and release could be achieved in multiple blue-light on/off cycles. As shown in Figure 3, the light-controlled client recruitment−release processes were repeated for at least three times, and the client mCherry fluorescence intensities were well retained during this time period without obvious photobleaching. Collectively, the LASC system could regulate the spatial organization of the client mCherry protein to condense in a reversible and repeatable manner by switching the blue light on and off.

Next, we investigated whether the LASC system could be used as an efficient platform to dynamically control the subcellular localization of functional proteins for cellular behavior regulation. We selected SulA as a model client, an endogenous protein of *E. coli* which interacts with the cell division protein FtsZ to inhibit the formation of Z ring and thus blocks the cell division to induce cell elongation.[28,29] It is deduced that the cell morphology can be manipulated by regulating the intracellular localization of SulA with blue light or in darkness (Figure 4a). Specifically, under blue light illumination, SulA can be recruited into the condensates, thereby preventing its binding to FtsZ and promoting the formation of the Z ring, ultimately resulting in normal cell division and the development of a rod-shaped morphology. Conversely, in the absence of blue light stimulation, SulA would remain in the cytoplasm, where it can freely interact with FtsZ. This interaction disrupts the formation of the Z ring, leading to abnormal cell division and elongation.

To test the above hypothesis, the recombinant cells co-expressing mtsSspBI8 and SulA-iLID were cultured in LB medium at 30 °C for 4 h either in the darkness or in the presence of blue light. According to TEM imaging (Figure S9), formation of multiple micron-sized condensates along the cell long axis was clearly observed. Microscopic observations showed that the cells maintained a rod-like shape when incubated under continuous blue light, whereas a filamentous morphology was observed for the cells under darkness (Figure 4b). Quantitative measurements of cell length showed a significant increasing trend in the cells cultured in darkness with 50% of the cells being >15 μm in length (Figure 4c). It should be noted that the cells cultured for 4 h in blue light were slightly longer than the cells before induction (Figure 4c). This might be due to the fact that formation of the synthetic condensates was time-dependent (Figure S1), and during the early stage, the nascent SulA-iLID fusion protein dispersed in the cytosol may have exerted an inhibitory effect on cell division; however, we cannot exclude the possibility that incomplete capture of SulA-iLID into the synthetic condensates might contribute to the partial inhibition of cell division. When the recombinant cells co-expressing mtsSspBI8 and SulA-iLID were cultured in the LB medium at 37 °C, the blue light irradiation also rescued the cell morphology, which verified functioning of the LASC system irrespective of the cell culture temperatures tested (Figure S10). To exclude the possibility that the formation of condensates solely would impact the cell morphology, the recombinant cells expressing the mtsSspBI8 scaffold (without client SulA expression) were similarly cultured and imaged. As these cells did not show significant differences in the cell length under light on and off conditions (Figure S11), neither the blue light nor the mtsSspBI8 condensate formation would affect the normal cell morphology. Furthermore, it was found that SspB binding to SulA-iLID alone was insufficient to inhibit SulA function (Figure S12), suggesting that the presence of the intact scaffold mtsSspBI8 and the resulting condensates was necessary for the blue light-triggered sequestration of SulA-iLID. Collectively, the above results proved that light-triggered recruitment of SulA into the condensates sequestered its inhibitory function and rescued the normal cell division and rod-shape morphology.

Lastly, we explored whether the light-switchable LASC system could support the dynamic control of the cell morphology in a reversible manner. To this end, the recombinant cells, co-expressing mtsSspBI8 and SulA-iLID,

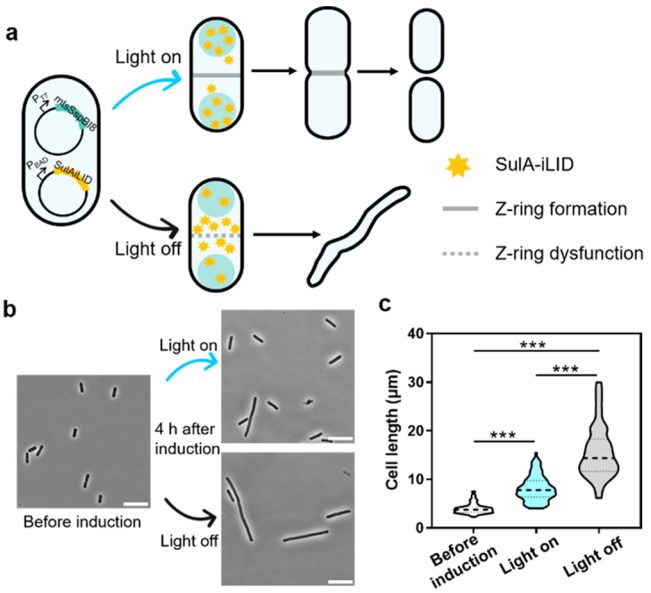

Figure 4. Light-triggered SulA recruitment and sequestration into synthetic condensates rescued normal cell division and morphology. (a) Illustration of the genetic constructs for cell morphology control by regulating the subcellular localization of SulA-iLID by switching blue light on and off. Under blue light, SulA-iLID was recruited to the mtsSspBI8 condensates and prevented from interaction with FtsZ, so that cells divided normally and formed rod shapes. Conversely, under the light off condition, SulA-iLID was dispersed in the cell cytosol and interacted with FtsZ to prevent Z-ring formation, so that cell division was inhibited to form an elongated filamentous shape. (b) Representative phase-contrast images of the *E. coli* cells co-expressing mtsSspBI8 and SulA-iLID cultured in LB medium and 30 °C under light on/off conditions for 4 h. Scale bars: 10 μm. (c) Quantification of the cell length from 8 to 10 fields of view in (b) containing 100 cells. Shown are violin plots with dashed and dotted lines indicating the median and interquartile values, respectively. Statistical significance was determined using Kruskal−Wallis test for *P* values (***$P < 0.001$). Data in parts b and c are representative of $n = 3$ independent experiments.

https://doi.org/10.1021/jacsau.4c00017
JACS Au 2024, 4, 1480−1488

were cultured with alternate light on−off−on−off cycles. In principle, the recombinant cells were first cultured in the presence of blue light for 4 h to recruit SulA-iLID into condensates for normal cell division; next, the cells were transferred to constant dark conditions in fresh medium for 2 h to release SulA-iLID from the condensates into the cytosol for blocking cell division; then the cells were illuminated with blue light again to sequester SulA-iLID into the condensates; finally, the cells were cultured in the darkness for the condensates to release SulA-iLID for a second time (Figure 5a). The imaging

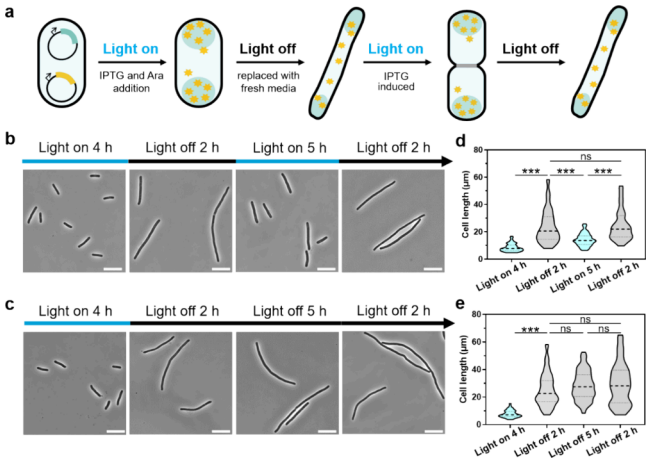

Figure 5. Dynamic control of cell morphology by light-switchable organization of cell division inhibitor SulA in synthetic condensates. (a) Schematic illustration of the design rationale for regulating cell shapes with light switching on/off repetitively during the cell culture. (b, c) Representative phase-contrast images of the cells co-expressing mtsSspBI8 and SulA-iLID cultured by light on−off−on−off cycles (b) and light on−off−off−off cycles (c), which serve as a negative control for comparison. Scale bars: 10 μm. (d, e) Quantification of the cell length from 8 to 10 fields of view of the cells (n = 100) as shown in (b) and (c). Shown are violin plots with dashed and dotted lines indicating the median and interquartile values, respectively. Statistical significance was determined using Kruskal−Wallis test for P values (ns, not significant; ***P < 0.001). Data in parts b−e are representative of n = 3 independent experiments.

results showed that the cells were remarkably elongated from the normal rod to the filamentous shape with a significant increase in cell length as the blue light switched from ON to OFF. And upon blue light illumination again, the cells became shorter to the essentially normal length resulting from normal division, and the cyclic alternation in cell morphology was realized by the blue light switching ON and OFF for two cycles (Figures 5b and 5d). In contrast, the control cells maintained an elongated shape under the continuous light off condition (Figures 5c and 5e). These results proved that it is possible to dynamically regulate the cell division in a reversible manner by light-induced recruitment and release of SulA from synthetic condensates in *E. coli*. Therefore, the LASC system appeared to be an ideal platform for cellular behavior control by spatiotemporal organization of the responsible client proteins.

For the light-switchable condensation system developed in the current study, its performance was evaluated on a 6-well plate with a culture volume of 2 mL. It would be interesting to explore in future studies the application of this optogenetic condensation system in shake flasks and bioreactors at the liter and larger scales. In addition, as the optogenetic condensation system can be readily expanded to condense and release alternative protein cargoes, such as metabolic pathway enzymes, transcription, and signaling factors, our work reinforces the perspective that the creation of designer membraneless organelles promises to be a fruitful area of future research.

CONCLUSION

In this work, we successfully designed and engineered a LASC system in model prokaryotic cells. This light-switchable system relies on the combination of iLID-SspB optical dimers and the synthetic condensates formed by phase separation of a disordered silk-like protein. The LASC system is capable of recruiting clients into the synthetic condensates rapidly at the submicron scale with high spatiotemporal precision in *E. coli*. Meanwhile, the client recruitment and release processes are also reversible and repeatable by switching the blue light on and off. Furthermore, the utility of the LASC system has been proof-of-demonstrated in dynamic cellular behavior control by subcellular organization of the cell division inhibitor SulA. Therefore, the presented LASC system helps to deepen the understanding of formation and functionalization of synthetic condensates in prokaryote cells, and due to its rapid, reversible, and repeatable nature, it also opens up a new way for dynamic control of cellular processes with great potential for applications in chemical and synthetic biology.

METHODS

Plasmid Construction

All plasmids and oligonucleotide primers used are listed in Tables S1 and S2. *E. coli* DH5α was used for cloning and plasmid propagation. The cells were grown in selective Luria−Bertani (LB) broth or LB plates with 1.5 wt % agar. The selection antibiotics were added at the following concentrations: 100 μg/mL ampicillin (Am), 30 μg/mL chloramphenicol (Cm), and 50 μg/mL kanamycin (Km). The DNA sequences encoding iLID and SspB (Micro)[20] were synthesized by Sangon Biotech (Shanghai, China) with codon optimized for expression in *E. coli* and cloned into pUC57 and pACYCDuet-1, termed pUC-iLID and pACYC-SspB(Micro), respectively. All DNA fragments amplified by PCR were completely sequenced after cloning.

Plasmids for the expression of scaffold proteins were constructed as follows. First, the DNA fragment encoding yellow fluorescent protein (YFP) was amplified from plasmid pRset-YFP with primers FYFPSpe and RYFPBam. The amplified fragment was digested with restriction enzymes *Spe*I-HF and *Bam*HI-HF and ligated with *Spe*I-*Bam*HI-digested pET28a4-MaSpI8 plasmid that was constructed previously,[14] resulting in plasmid pET28a4-I8YFP. Besides, a flexible linker, $(GGS)_4$, was added between YFP and MaSpI8. This linker was also used in the protein fusion described in the next part of this section. Then, the DNA fragment encoding SspB was amplified from plasmid pACYC-SspB(Micro) with the primers FSspBNde and RSspBNhe. The amplified fragment was digested by *Nde*I and *Nhe*I-HF and ligated with *Nde*I-*Nhe*I-digested pET28a4-MaSpI8 plasmid, resulting in plasmid pET28a4-SspBI8. The restricted fragment of SspB was also cloned into plasmid pET28a4-I8YFP to construct plasmid pET28a4-SspBI8YFP. The DNA fragment encoding membrane targeting sequence (mts) was obtained by annealing the oligonucleotides FmtsNde and RmtsNco and directly ligated with the *Nco*I-*Nde*I-digested pET28a4-SspBI8 to make plasmid pET28a4-mtsSspBI8. For the expression of YFP-tagged mtsSspBI8, plasmid pET28a4-mtsSspBI8 was digested with *Nco*I-HF and *Spe*I-HF, and the resulting 1.2-kb mtsSspBI8 fragment was inserted into pET28a4-I8YFP at the same sites to make plasmid pET28a4-mtsSspBI8YFP. The mtsSspBI8 fragment, treated with *Nco*I-HF and *Bam*HI-HF, was also ligated into plasmid pACYCDuet-1 at the same sites to make plasmid pACYC-mtsSspBI8. For the expression of YFP-tagged SspB, the DNA fragment encoding YFP was amplified from pRset-YFP with the

https://doi.org/10.1021/jacsau.4c00017
JACS Au 2024, 4, 1480−1488

primers FYFPNhe and RYFPXho. The amplified fragment was digested by *Nhe*I-HF and *Xho*I and cloned into plasmid pET28a4-SspBI8 at the same sites to make plasmid pET28a4-SspBYFP. The aforementioned pET28a4-derived plasmids allowed expression of the respective scaffold proteins under the T7 promoter, which is inducible by isopropyl-β-D-thiogalactoside (IPTG).

For constitutive expression of the client protein mCherry-iLID, we first constructed an intermediate plasmid pACYC-mCherryiLID. Primers FmChBam and RmChHind were used to amplify the fragment encoding mCherry from plasmid pACYC-I16-rfp, which was constructed as described previously.[13] The iLID fragment was amplified from plasmid pUC-iLID with the primers FiLIDHind and RiLIDXho. The amplified fragment of mCherry was digested by *Bam*HI-HF and *Hin*dIII-HF and ligated with *Bam*HI-*Hin*dIII digested pACYCDuet-1 vector, resulting in pACYC-mCherry. The amplified fragment of iLID was digested with *Hin*dIII-HF and *Xho*I, and the restricted fragment of iLID was cloned into plasmid pACYC-mCherry at the same sites to yield plasmid pACYC-mCherryiLID. Then, the primers FmChiLKpn and RmChiLBamH were used to amplify the fragment of mCherry-iLID. The amplified fragment was digested by *Kpn*I-HF and *Bam*HI-HF and cloned into a laboratory stock plasmid pZA16-mCherry at the same sites, resulting in plasmid pZA16-mCherryiLID. To construct an empty expression vector, plasmid pZA16 was made by deleting the *mCherry* gene fragment from plasmid pZA16-mCherry, which was used as a template to perform an inverse PCR with primers FZA16 and RZA16. The PCR product was then self-ligated to generate pZA16.

For inducible expression of the SulA-iLID, the DNA fragment encoding SulA was amplified from the genomic DNA of *E. coli* MG1655 with primers FsulANhe and RsulAXho, and the DNA fragment encoding iLID was amplified from plasmid pUC-iLID with primers FiLIDXho and RiLIDKpn. Then, the amplified *sulA* fragment was digested by *Nhe*I-HF and *Xho*I, and the iLID fragment was digested with *Xho*I and *Kpn*I-HF. These two restricted fragments were mixed and ligated with the *Nhe*I-*Kpn*I fragment of expression vector pBAD-HisA (Invitrogen, Carlsbad, CA). The resulting plasmid pBAD-SulAiLID allowed expression of the cargo protein SulA-iLID under the arabinose-inducible *araBAD* promoter.

Bacterial Strains and Culture Condition

For confocal fluorescence imaging and light illumination studies, recombinant cells of *E. coli* BL21(DE3) transformed with intended plasmids were cultured overnight in 4 mL of LB with antibiotics at 37 °C and 220 rpm in a shaking incubator. Then, 200 μL overnight cultures were diluted in 20 mL of LB medium with appropriate antibiotics in a 250 mL flask and grown at 37 °C and 220 rpm. When the cell optical density at 600 nm (OD_{600}) reached 0.5−0.6, cells were induced with 25 μM IPTG (unless otherwise specified) at 30 °C for protein expression. Notably, for the light illumination experiment, the cells were cultured with aluminum foil to avoid the daylight. Samples were taken 6 h after induction for confocal microscopy and TEM analyses. In another experimental setup, the recombinant *E. coli* cells were grown in flasks with the minimal R/2 medium[30] supplemented with 4 g/L glucose. When the cell OD_{600} reached 0.5−0.6, the cells were similarly treated with IPTG at 30 °C for 6 h and then sampled for microscopic analysis.

For cell morphology assay, recombinant cells of *E. coli* BL21(DE3) co-transformed with plasmids pACYC-mtsSspBI8 and pBAD-SulAiLID were cultured in 250 mL flasks containing 20 mL of LB medium at 37 °C and 220 rpm. When the cell OD_{600} reached 0.5−0.6, cells were induced with 100 μM IPTG and 0.2% arabinose. Then, the cultures were transferred into 6-well plates (2 mL in each well) and grown at 30 °C and 150 rpm for 4 h under blue light and darkness, respectively. To dynamic control the cell morphology, the recombinant cells were induced with 100 μM IPTG and 0.2% (w/v) arabinose at an OD_{600} of 0.5−0.6; then 2 mL cultures were transferred into 6-well plates and grown at 30 °C and 150 rpm under blue light for 4 h. Next, the culture medium was removed and replaced with 2 mL of fresh selective LB medium without inducers, and the cells were grown at 30 °C and 150 rpm under darkness (wrapped with aluminum foil) for 2 h. Notably, 0.2% (w/v) glucose was additionally supplemented into the cell cultures to prevent leaky expression from the *araBAD* promoter. After 2 h of dark cultivation, the cultures were re-exposed to blue light conditions for 5 h following induction with 100 μM IPTG. Finally, the cell cultures were transferred back to the darkness for an additional 2 h. Alternatively, the cells were continuously cultured in the darkness (without the exposure to the second blue light illumination) as a control. Samples for the morphology observation were taken at the indicated time points.

Microscopy Imaging and In Situ Blue Light Illumination Assay

The confocal imaging and light illumination experiment of *E. coli* cells was performed using the Leica TCS SP8 STED 3X microscope (Leica Microsystems). Recombinant cells expressing fluorescent proteins were collected by centrifugation at 1503*g* for 5 min at 23 °C. After washing twice with PBS, 5 μL of cell samples suspended in PBS was then placed on glass slides for confocal imaging. The specimens were illuminated with a 514 nm laser for yellow fluorescent protein and a 561 nm laser for mCherry fluorescent protein.

For light illumination assay, recombinant cells co-expressing mtsSspBI8 and mCherry-iLID were collected by centrifugation at 1503*g* for 5 min at 23 °C. Samples were resuspended and diluted in PBS to an OD_{600} of ∼0.2 and transferred (1.5 μL) to 1.5% (w/v) low melting agarose pads freshly prepared with phosphate buffered saline. Blue light illumination was performed with a 488 nm laser line (Ar laser; output power 65 mW, 50% acousto-optic tunable filter).

For cell morphology imaging, the cell cultures (∼5 μL) were placed on glass slides for observation. Morphology images were performed using a phase-contrast Nikon Eclipse Ti-2E inverted microscope equipped with a Nikon Plan Apo 100× Oil Ph3 DM (NA 1.45) objective lens and controlled by NIS-Elements AR 5.20.00 software.

Light Compartment Setup

For cell culture under light illumination, the 6-well plate was placed onto a blue LED array panel (450−455 nm) with an adjustable current source. The light intensity was turned to a range from 90 to 100 μmol m^{-2} s^{-1}, measured using a LI-250A light meter equipped with a LI-190SA quantum sensor (LI-COR Biosciences).

Transmission Electron Microscopy (TEM)

TEM imaging of the *E. coli* cells was conducted using a Tecnai G2 Spirit BioTWIN transmission electron microscope (FEI Company) equipped with a Gatan 832 CCD camera (Gatan). The cells were collected by centrifugation at 1503*g* for 5 min at 23 °C, and the samples were washed three times with deionized water and then resuspended in deionized water. Ten microliters of the cell suspension was dropped onto a carbon-coated copper grid for 20 min at room temperature. The excess liquid was blotted off with filter paper, and the grid was then air-dried and examined under a transmission electron microscope.

SDS-PAGE Analysis

Briefly, the collected cells were suspended in 10 mM Tris-HCl buffer (pH 7.5) containing 2 mM EDTA, mixed with a 5× Laemmli sample buffer, and then boiled. After centrifugation, the supernatant was loaded onto 10% SDS-PAGE gels for electrophoresis. The gels were stained with Coomassie Brilliant Blue R250 and scanned by using a Microtek Bio-5000 Plus scanner (Microtek).

Image Analysis

The fluorescence intensity of the condensates to cytosol ratio was quantified using ImageJ software. Briefly, the cell shapes were first determined from bright field microscopy images, and the condensates were inferred based on mCherry fluorescence distribution within the cells. Then the confocal images were converted to 8-bit grayscale images and background-subtracted. The mean fluorescence intensity of condensate was determined by the average pixel intensity in the condensate area (I_{cond}) and the cytosolic region (I_{cyto}). Then the condensate-to-cytosol intensity ratio was calculated as the mean fluorescence intensity of condensate divided by the mean fluorescence

https://doi.org/10.1021/jacsau.4c00017
JACS Au 2024, 4, 1480−1488

intensity of cytosol (I_{cond}/I_{cyto}). For fluorescence distribution analysis, the fluorescence intensity profile along the medial axes of *E. coli* cell bodies was performed by using the Leica LASX software.

To quantify the cell length, ImageJ software was used to measure the distance of the cell bodies from one pole to the other. In the fields, only visible cells were measured.

Statistical Analysis

GraphPad Prism 8 was used for statistical analysis, and all data with statistics were derived from at least three biological replicates. To test the significance, an unpaired *t*-test was used for comparison between two groups, and a one-way ANOVA was used for comparison of more than two groups. For analysis of the recruitment and release kinetics of client mCherry-iLID, the curves were fit with one-phase exponential association and one-phase exponential decay in GraphPad Prism.

■ ASSOCIATED CONTENT

Supporting Information

The Supporting Information is available free of charge at https://pubs.acs.org/doi/10.1021/jacsau.4c00017.

> Plasmids and oligonucleotide primers used, condensate formation with induction time, TEM imaging of the cells, confocal microscopy images, SDS-PAGE analysis, reversible client recruitment and release in a 1 min light on/off cycle, light responsiveness of the cells co-expressing mtsSspBI8 and mCherry, functioning of the LASC system at 37 °C to rescue cell morphology, and morphology of the control cells expressing mtsSspBI8 and those co-expressing SspB(micro) and SulA-iLID (Tables S1−S2 and Figures S1−S12) (PDF)

■ AUTHOR INFORMATION

Corresponding Authors

Zhi-Gang Qian − *State Key Laboratory of Microbial Metabolism, Joint International Research Laboratory of Metabolic & Developmental Sciences, School of Life Sciences and Biotechnology, Shanghai Jiao Tong University, Shanghai 200240, China;* orcid.org/0000-0002-0133-0605; Email: zgqian@sjtu.edu.cn

Xiao-Xia Xia − *State Key Laboratory of Microbial Metabolism, Joint International Research Laboratory of Metabolic & Developmental Sciences, School of Life Sciences and Biotechnology, Shanghai Jiao Tong University, Shanghai 200240, China;* orcid.org/0000-0001-8375-1616; Email: xiaoxiaxia@sjtu.edu.cn

Authors

Fang Pan − *State Key Laboratory of Microbial Metabolism, Joint International Research Laboratory of Metabolic & Developmental Sciences, School of Life Sciences and Biotechnology, Shanghai Jiao Tong University, Shanghai 200240, China*

Han Zu − *State Key Laboratory of Microbial Metabolism, Joint International Research Laboratory of Metabolic & Developmental Sciences, School of Life Sciences and Biotechnology, Shanghai Jiao Tong University, Shanghai 200240, China*

Ya-Jiao Zhu − *State Key Laboratory of Microbial Metabolism, Joint International Research Laboratory of Metabolic & Developmental Sciences, School of Life Sciences and Biotechnology, Shanghai Jiao Tong University, Shanghai 200240, China*

Complete contact information is available at: https://pubs.acs.org/10.1021/jacsau.4c00017

Notes

The authors declare no competing financial interest.

■ ACKNOWLEDGMENTS

Financial support was provided by the National Key Research and Development Program of China (Grant 2020YFA0907702 to X.-X.X.), the National Natural Science Foundation of China (Grants 32270107 and 22075179 to Z.-G.Q. and 32071414 to X.-X.X.), and the Natural Science Foundation of Shanghai (21ZR1432100 to Z.-G.Q.).

■ REFERENCES

(1) Banani, S. F.; Lee, H. O.; Hyman, A. A.; Rosen, M. K. Biomolecular Condensates: Organizers of Cellular Biochemistry. *Nat. Rev. Mol. Cell Biol.* **2017**, *18* (5), 285−298.

(2) Boeynaems, S.; Alberti, S.; Fawzi, N. L.; Mittag, T.; Polymenidou, M.; Rousseau, F.; Schymkowitz, J.; Shorter, J.; Wolozin, B.; Van Den Bosch, L.; Tompa, P.; Fuxreiter, M. Protein Phase Separation: A New Phase in Cell Biology. *Trends Cell Biol.* **2018**, *28* (6), 420−435.

(3) Staples, M. I.; Frazer, C.; Fawzi, N. L.; Bennett, R. J. Phase Separation in Fungi. *Nat. Microbiol* **2023**, *8* (3), 375−386.

(4) Zhang, H.; Ji, X.; Li, P. L.; Liu, C.; Lou, J. Z.; Wang, Z.; Wen, W. Y.; Xiao, Y.; Zhang, M. J.; Zhu, X. L. Liquid-liquid Phase Separation in Biology: Mechanisms, Physiological Functions and Human Diseases. *Sci. China Life Sci.* **2020**, *63* (7), 953−985.

(5) Azaldegui, C. A.; Vecchiarelli, A. G.; Biteen, J. S. The Emergence of Phase Separation as an Organizing Principle in Bacteria. *Biophys. J.* **2021**, *120* (7), 1123−1138.

(6) Lyon, A. S.; Peeples, W. B.; Rosen, M. K. A Framework for Understanding the Functions of Biomolecular Condensates across Scales. *Nat. Rev. Mol. Cell Biol.* **2021**, *22* (3), 215−235.

(7) Gao, Z.; Yuan, J.; He, X.; Wang, H.; Wang, Y. Phase Separation Modulates the Formation and Stabilities of DNA Guanine Quadruplex. *JACS Au* **2023**, *3* (6), 1650−1657.

(8) Ditlev, J. A.; Case, L. B.; Rosen, M. K. Who's In and Who's Out—Compositional Control of Biomolecular Condensates. *J. Mol. Biol.* **2018**, *430* (23), 4666−4684.

(9) Zhao, E. M.; Suek, N.; Wilson, M. Z.; Dine, E.; Pannucci, N. L.; Gitai, Z.; Avalos, J. L.; Toettcher, J. E. Light-Based Control of Metabolic Flux through Assembly of Synthetic Organelles. *Nat. Chem. Biol.* **2019**, *15* (6), 589−597.

(10) Yoshikawa, M.; Yoshii, T.; Ikuta, M.; Tsukiji, S. Synthetic Protein Condensates That Inducibly Recruit and Release Protein Activity in Living Cells. *J. Am. Chem. Soc.* **2021**, *143* (17), 6434−6446.

(11) Jain, A.; Vale, R. D. RNA Phase Transitions in Repeat Expansion Disorders. *Nature* **2017**, *546* (7657), 243−247.

(12) Zhou, P.; Liu, H.; Meng, X.; Zuo, H. Y.; Qi, M. Y.; Guo, L.; Gao, C.; Song, W.; Wu, J.; Chen, X. L.; Chen, W.; Liu, L. M. Engineered Artificial Membraneless Organelles in *Saccharomyces cerevisiae* to Enhance Chemical Production. *Angew. Chem., Int. Ed.* **2023**, *62* (14), No. e202215778.

(13) Wei, S. P.; Qian, Z. G.; Hu, C. F.; Pan, F.; Chen, M. T.; Lee, S. Y.; Xia, X. X. Formation and Functionalization of Membraneless Compartments in *Escherichia coli*. *Nat. Chem. Biol.* **2020**, *16* (10), 1143−1148.

(14) Chen, M. T.; Hu, C. F.; Huang, H. B.; Qian, Z. G.; Xia, X. X. Spatially Directed Biosynthesis of Quantum Dots via Spidroin Templating in *Escherichia coli*. *Angew. Chem., Int. Ed.* **2022**, *61* (49), No. e202214177.

(15) Wang, Y.; Liu, M.; Wei, Q. X.; Wu, W. J.; He, Y. P.; Gao, J. Y.; Zhou, R. J.; Jiang, L. W.; Qu, J. N.; Xia, J. Phase-Separated

Multienzyme Compartmentalization for Terpene Biosynthesis in a Prokaryote. *Angew. Chem., Int. Ed.* **2022**, *61* (29), No. e202203909.
(16) Wan, L.; Zhu, Y. Y.; Zhang, W. L.; Mu, W. M. Phase-Separated Synthetic Organelles Based on Intrinsically Disordered Protein Domain for Metabolic Pathway Assembly in *Escherichia coli*. *ACS Nano* **2023**, *17* (11), 10806−10816.
(17) Dai, Y. F.; Farag, M.; Lee, D.; Zeng, X. Z.; Kim, K.; Son, H. I.; Guo, X.; Su, J.; Peterson, N.; Mohammed, J.; Ney, M.; Shapiro, D. M.; Pappu, R. V.; Chilkoti, A.; You, L. C. Programmable Synthetic Biomolecular Condensates for Cellular Control. *Nat. Chem. Biol.* **2023**, *19* (4), 518−528.
(18) Huang, Z. K.; Sun, L. Z.; Lu, G. Z.; Liu, H. R.; Zhai, Z. H.; Feng, S. T.; Gao, J.; Chen, C. Y.; Qing, C. H.; Fang, M.; Chen, B. W.; Fu, J. L.; Wang, X.; Chen, G. Q. Rapid Regulations of Metabolic Reactions in *Escherichia coli* via Light-Responsive Enzyme Redistribution. *Biotechnol. J.* **2022**, *17* (9), 2200129.
(19) Zhou, X. X.; Fan, L. L. Z.; Li, P. P.; Shen, K.; Lin, M. Z. Optical Control of Cell Signaling by Single-Chain Photoswitchable Kinases. *Science* **2017**, *355* (6327), 836−842.
(20) Guntas, G.; Hallett, R. A.; Zimmerman, S. P.; Williams, T.; Yumerefendi, H.; Bear, J. E.; Kuhlman, B. Engineering an Improved Light-Induced dimer (iLID) for Controlling the Localization and Activity of Signaling Proteins. *Proc. Natl. Acad. Sci. U. S. A.* **2015**, *112* (1), 112−117.
(21) Qian, Z. G.; Huang, S. C.; Xia, X. X. Synthetic Protein Condensates for Cellular and Metabolic Engineering. *Nat. Chem. Biol.* **2022**, *18* (12), 1330−1340.
(22) Nadendla, K.; Simpson, G. G.; Becher, J.; Journeaux, T.; Cabeza-Cabrerizo, M.; Bernardes, G. J. L. Strategies for Conditional Regulation of Proteins. *JACS Au* **2023**, *3* (2), 344−357.
(23) Zimmerman, S. P.; Hallett, R. A.; Bourke, A. M.; Bear, J. E.; Kennedy, M. J.; Kuhlman, B. Tuning the Binding Affinities and Reversion Kinetics of a Light Inducible Dimer Allows Control of Transmembrane Protein Localization. *Biochemistry* **2016**, *55* (37), 5264−5271.
(24) Wah, D. A.; Levchenko, I.; Baker, T. A.; Sauer, R. T. Characterization of a Specificity Factor for an AAA+ ATPase: Assembly of SspB Dimers with SsrA-Tagged Proteins and the ClpX Hexamer. *Chem. Biol.* **2002**, *9* (11), 1237−1245.
(25) Hu, Z. L.; Lutkenhaus, J. A Conserved Sequence at the C-terminus of MinD is Required for Binding to the Membrane and Targeting MinC to the Septum. *Mol. Microbiol.* **2003**, *47* (2), 345−355.
(26) Protter, D. S. W.; Rao, B. S.; Van Treeck, B.; Lin, Y.; Mizoue, L.; Rosen, M. K.; Parker, R. Intrinsically Disordered Regions Can Contribute Promiscuous Interactions to RNP Granule Assembly. *Cell Reports* **2018**, *22* (6), 1401−1412.
(27) Krishnan, R.; Ranganathan, S.; Maji, S. K.; Padinhateeri, R. Role of Non-Specific Interactions in the Phase-Separation and Maturation of Macromolecules. *PLoS Comput. Biol.* **2022**, *18* (5), No. e1010067.
(28) Chen, Y. D.; Milam, S. L.; Erickson, H. P. SulA Inhibits Assembly of FtsZ by a Simple Sequestration Mechanism. *Biochemistry* **2012**, *51* (14), 3100−3109.
(29) Vedyaykin, A.; Rumyantseva, N.; Khodorkovskii, M.; Vishnyakov, I. SulA is Able to Block Cell Division in *Escherichia coli* by a Mechanism Different from Sequestration. *Biochem. Biophys. Res. Commun.* **2020**, *525* (4), 948−953.
(30) Yang, Y. X.; Qian, Z. G.; Zhong, J. J.; Xia, X. X. Hyper-production of large proteins of spider dragline silk MaSp2 by *Escherichia coli* via synthetic biology approach. *Process Biochem.* **2016**, *51* (4), 484−490.

https://doi.org/10.1021/jacsau.4c00017
JACS Au 2024, 4, 1480−1488